IEEE Access
Multidisciplinary | Rapid Review | Open Access Journal

Received April 30, 2018, accepted June 27, 2018, date of publication July 5, 2018, date of current version July 30, 2018.

Digital Object Identifier 10.1109/ACCESS.2018.2853111

Compressive-Sensing-Based Simultaneous Polarimetric HRRP Reconstruction With Random OFDM Pair Radar Signal

QIHUA WU[1], FENG ZHAO[1], XIA AI[2], XIAOFENG AI[1], JIN LIU[1], AND SHUNPING XIAO[1]

[1]State Key Laboratory of Complex Electromagnetic Environment Effects on Electronics and Information System, National University of Defense Technology, Changsha 410073, China

[2]National Key Laboratory of Science and Technology on Test Physics and Numerical Mathematics, Beijing 100000, China

Corresponding author: Xiaofeng Ai (anxifu2001@163.com)

This work was supported by the National Natural Science Foundation of China under Grant 61101180, Grant 61401491, and Grant 61490690.

ABSTRACT Orthogonal waveform design is of great significance for simultaneous polarimetric high-resolution range profile (HRRP) reconstruction. In this paper, a novel waveform called a random orthogonal frequency division multiplexing (R-OFDM) pair is proposed. The proposed signal exploits ideal orthogonality by randomly selecting different subsets of a full-band OFDM signal. The compressive sensing (CS) technique is applied for HRRP reconstruction due to the sparse property of the proposed waveform. To further utilize the information of different polarization channels, the joint CS reconstruction algorithm called a fully polarization-simultaneous orthogonal matching pursuit (FP-SOMP) is proposed instead of the single polarization-OMP algorithm by exploiting row-sparsity of different polarization channels. Both numerical simulations and measured unmanned aerial vehicle data experiments demonstrate that the R-OFDM pair and the CS-based FP-SOMP algorithm are qualified for simultaneous polarimetric HRRP reconstruction.

INDEX TERMS Simultaneous polarimetric radar, high-resolution range profile (HRRP), orthogonal frequency division multiplexing (OFDM), compressive sensing (CS).

I. INTRODUCTION

Both high resolution and polarimetric information contribute to target recognition in remote sensing applications. The high resolution information involves geometrical characteristic such as length, size and shape of target. The polarization information describes the roughness of target surface, degree of symmetry and so on, which is widely applied in target detection, target recognition and parameter estimation. Thus the combination of high resolution and polarization attracts great attention in the past decades [1], [2].

The polarimetric high-resolution range profile (HRRP) syntheses involve two independent procedures: one is to obtain the HRRP with wideband signals such as stepped frequency wave(SFW) and wideband linear frequency modulation(LFM) signal. The other is to obtain the whole polarization channel data with fully polarimetric measurements. Currently, alternate polarimetric measurement (APM) is mainly adopted [3], [4]. The polarizations are alternately switched between the horizontal and vertical polarizations on transmission and reception. As a result, the polarimetric HRRPs are obtained in a sequence of two measurements. For high dynamic targets, the relative position between target and radar has changed during two measurements. Thus the polarimetric HRRPs cannot be accurately measured. Instead of APM, simultaneous polarimetric measurement(SPM) has been proposed. By simultaneously transmitting and receiving orthogonal polarimetric wave, the polarimetric HRRPs are obtained within one transmitting period. In this case, pulse-to-pulse based switching of transmitting polarizations can be avoided. Due to simultaneous transmission and reception, the signals must be orthogonal in either time domain or frequency domain. Frequency shifted pulses, pairs of up-down slope LFM signals and phased coded modulation(PCM) signals are widely applied in SPM [5]–[7].

Orthogonal Frequency Division Multiplexing (OFDM) technique is widely applied in communication [8], which also attracts great attention in radar applications for its multi-carrier spread-spectrum property. Radar systems utilizing OFDM techniques are reported in [9] and [10]. Recently, interleaved-OFDM(I-OFDM) pair is proposed to raise the

cross-channel isolation level in narrow-band SPM applications by utilizing the orthogonality of sub-carriers of OFDM signals [11]. By alternately sampling from the same full-band OFDM signal, the wave pair yields theoretical orthogonality in frequency domain. Thus the isolation limitation of pairs of up-down slope wide-band LFM signal can be overcome. However, the unambiguous range of I-OFDM pair is half of full-band OFDM signal due to the interleaved sampling. When it comes to wide-band simultaneous polarimetric HRRP reconstruction applications, the HRRPs of targets with relatively large length in the line of sight(LOS) of radar may be coupled. Besides, the discrete Fourier transform(DFT)-based processing algorithm proposed in [11] is applied to each polarization channel individually, which does not utilize the links among different polarizations.

Recently, applications of sparse signals by randomly selecting limited parts of the complete waveform based on compressive sensing (CS) theory are discussed in [12] and [13]. According to CS theory, the exact recovery of an unknown sparse signal can be obtained from limited measurements by solving a sparsity-constrained optimization problem [14]–[19]. Inspired by this, random-OFDM (R-OFDM) pair is proposed by randomly selecting orthogonal subsets of the full-band OFDM signal in this paper. By this way, the same unambiguous range as the full-band OFDM signal is obtained for each R-OFDM signal. Then the classic CS-based processing algorithm called Single Polarization-Orthogonal Matching Pursuit (SP-OMP) is applied to reconstruct the polarimetric HRRPs. Moreover, to fully utilize the information among different polarization channels, the Fully Polarization-Simultaneous OMP(FP-SOMP) algorithm is further proposed. Then the polarimetric HRRPs are reconstructed more accurately and robustly.

The remainder of the paper is as follows. Section II presents the signal model of R-OFDM pair. Then in Section III the two CS-based processing algorithms called SP-OMP and FP-SOMP are detailedly presented. Numerical simulations and measured unmanned aerial vehicle(UAV) data experiments are separately conducted to demonstrate the validity of the proposed method in Section IV and Section V. Section VI ends with conclusions and some future research directions.

II. SIGNAL MODEL

As shown in Fig.1(a), a full-band OFDM signal consists of a sequence of N narrowband subcarrriers with frequencies stepped from pulse to pulse. The frequencies are denoted as $f_n = f_0 + n\Delta f$, where $n = 0, 1, 2, \cdots, N-1$, f_0 is the carrier frequency, Δf is the frequency interval of adjacent pulses. The transmitted full-band OFDM signal is

$$x(t) = \sum_{n=0}^{N-1} \mathrm{rect}(t/\tau)\exp(j2\pi f_n t) \tag{1}$$

where t is the fast time variable with $-T/2 \le t \le T/2$, and T is the pulse repetition interval (PRI), τ is the sub-pulse

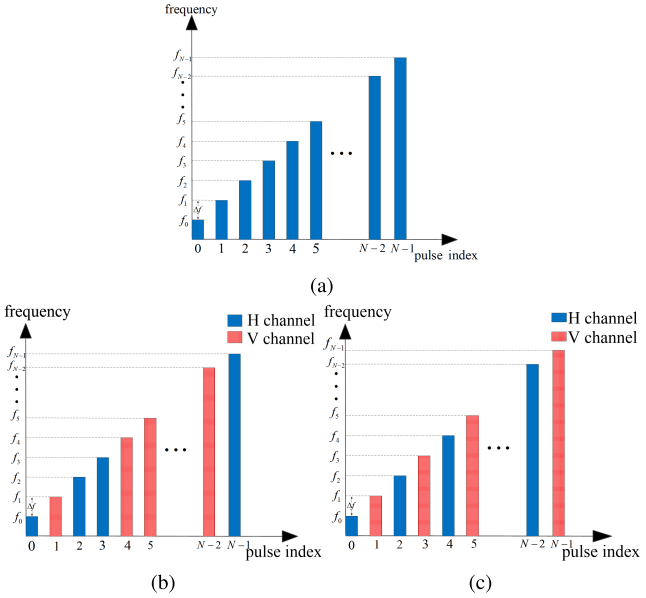

FIGURE 1. Signal model. (a)full-band OFDM signal. (b)R-OFDM pair. (c)I-OFDM pair.

width, and $\mathrm{rect}(t/\tau)$ equals to 1 when $|t/\tau| < 0.5$, otherwise $\mathrm{rect}(t/\tau) = 0$.

To achieve the orthogonality, the frequency interval should satisfy $\Delta f = m/\tau$ according to the properties of $\mathrm{sinc}(\cdot)$ function, where m is a positive integer [12]. Specially $\Delta f = 1/\tau$. The DFT-based algorithms can be applied for the echo processing [11]. The synthesized bandwidth is $B = N\Delta f$, the range resolution is $\Delta R = c/2B$, and the unambiguous range is $\Delta r = [-c/4\Delta f, c/4\Delta f]$, respectively, where c is the velocity of electromagnetic wave propagation.

In recent years, CS theory has been widely applied in imaging radar, which can reconstruct HRRPs with limited measurements that are randomly selected from the complete signal by utilizing the sparsity of radar targets. Inspired by CS theory, a novel R-OFDM pair radar signal is proposed by randomly selecting orthogonal sub-pulses from full-band OFDM signal for simultaneous polarimetric HRRP reconstruction.

As shown in Fig.1(b), the selected $N/2$ sub-pulses for R-OFDM pair are denoted by

$$f_{\mathrm{H}n} = f_0 + G_{\mathrm{H}}(n)\Delta f \tag{2}$$
$$f_{\mathrm{V}n} = f_0 + G_{\mathrm{V}}(n)\Delta f \tag{3}$$

where G_{H} and G_{V} are orthogonal subsets of $[0 : N-1]$ with $|G_{\mathrm{H}}| = |G_{\mathrm{V}}| = N/2$ and $G_{\mathrm{H}} \cup G_{\mathrm{V}} = [0 : N-1]$, n runs from 0 to $N/2-1$.

Thus R-OFDM pair can be written as

$$x_{\mathrm{H}}(t) = \sum_{n=0}^{N/2-1} \mathrm{rect}(t/\tau)\exp(j2\pi f_{\mathrm{H}n} t) \tag{4}$$
$$x_{\mathrm{V}}(t) = \sum_{n=0}^{N/2-1} \mathrm{rect}(t/\tau)\exp(j2\pi f_{\mathrm{V}n} t) \tag{5}$$

When the R-OFDM pair is transmitted, the signal for the orthogonal polarization channel is

$$x(t) = [x_{\mathrm{H}}(t), x_{\mathrm{V}}(t)]^T \tag{6}$$

Assume that the target involves P scatterers, R_p is the distance between the radar and pth scatterer with the polarization scattering matrix (PSM) $\mathbf{S}_p = \begin{bmatrix} S^p_{\mathrm{HH}} & S^p_{\mathrm{HV}} \\ S^p_{\mathrm{VH}} & S^p_{\mathrm{VV}} \end{bmatrix}$. Then the target echo can be given by

$$y(t) = [y_{\mathrm{H}}(t), y_{\mathrm{V}}(t)]^T \tag{7}$$

where

$$y_{\mathrm{H}}(t) = \sum_{p=1}^{P} (S^p_{\mathrm{HH}} x_{\mathrm{H}}(t-\tau_p) + S^p_{\mathrm{VH}} x_{\mathrm{V}}(t-\tau_p)) \tag{8}$$

$$y_{\mathrm{V}}(t) = \sum_{p=1}^{P} (S^p_{\mathrm{HV}} x_{\mathrm{H}}(t-\tau_p) + S^p_{\mathrm{VV}} x_{\mathrm{V}}(t-\tau_p)) \tag{9}$$

where $\tau_p = 2R_p/c$ denotes the time-delay of the pth scatterer.

Due to the orthogonality of OFDM sub-pulses, the co-polar and cross-polar R-OFDM echo can get separated by carrying out Fourier transform and indexing the sub-pulses denoted by $f_{\mathrm{H}n}$ and $f_{\mathrm{V}n}$ respectively after receving the fully polarization echo.

Fig.1(c) presents the I-OFDM pair signal proposed in [11] as a comparison. The sub-pulses are alternately selected from full-band OFDM signal, which are given by

$$f'_{\mathrm{H}n} = f_0 + 2n\Delta f \tag{10}$$

$$f'_{\mathrm{V}n} = f_0 + (2n+1)\Delta f \tag{11}$$

Comparing (10)(11) with (2)(3), the difference between the proposed R-OFDM pair and I-OFDM pair lies in the selection mechanism of sub-pulses, which uses the random selection instead of alternate selection for the proposed R-OFDM pair. As shown in Fig.1(c), it turns out to be a linear signal for each I-OFDM signal. Thus the DFT-based algorithm for full-band OFDM signal is still applicable for signal processing. However, the I-OFDM pair has two shortages. On the one hand, the frequency interval of each I-OFDM signal turns to be $\Delta f' = 2\Delta f$, thus the unambiguous range for I-OFDM pair is $\Delta r = [-c/8\Delta f, c/8\Delta f]$, which is half of full-band OFDM signal. Thus it may cause range ambiguity for targets with large length in the LOS of radar for polarimetric HRRP reconstruction. On the other hand, the DFT-based processing method processes the echo of each polarization channel individually. If the fully polarimetric information can be utilized more adequately, the accuracy of the polarimetric HRRPs will be further improved.

With the proposed R-OFDM pair, the minus frequency interval is still Δf as shown in Fig.1(b), hence the unambiguous range of each R-OFDM signal is the same as the full-band OFDM signal. Thus it is more applicable for polarimetric HRRP reconstruction. Besides, the anti-jamming performance may also greatly benefit due to the random property of the transmitting signal.

However, due to the randomness of the proposed waveform, DFT-based signal processing algorithm suitable for I-OFDM pair will generate high-level sidelobes and grating lobes. Hence, the CS-based algorithm is proposed for polarimetric HRRP reconstruction. Detailed analyses are presented in Section III.

III. POLARIMETRIC HRRP RECONSTRUCTION BASED ON CS THEORY

According to scattering theory, scattering properties of radar target can be regarded as the linear superposition of limited strong scatterers in high-frequency area. Thus the HRRP is formed by some discrete peak values for radar target. Hence the sparsity is satisfied for application of CS theory. Inspired by this, the CS-based algorithms are proposed for polarimetric HRRP reconstruction of the R-OFDM pair.

A. CS MODEL OF R-OFDM PAIR

For full-band OFDM signal, by carrying out Fourier transform to the received echo, coarse range profiles of each sub-pulse can be obtained as $e_d(i), i = 0, 1, \cdots, N-1$. The HRRP obtained by the original N sub-pulses is denoted as $h(k), k = 0, 1, \cdots, N-1$. Then

$$\mathbf{e}_d = \mathbf{\Psi}\mathbf{h} \tag{12}$$

where $\mathbf{e}_d = [e_d(0), e_d(1), \cdots, e_d(N-1)]^T$ is a $N \times 1$ vector of coarse range profiles, $\mathbf{h} = [h(0), h(1), \cdots, h(N-1)]^T$ is a $N \times 1$ vector of HRRP sequence. $\mathbf{\Psi}$ is a $N \times N$ IFFT dictionary matrix, which is given by

$$\mathbf{\Psi} = \begin{bmatrix} 1 & 1 & 1 & \cdots & 1 \\ 1 & W_N^{-1} & W_N^{-2} & \cdots & W_N^{-(N-1)} \\ 1 & W_N^{-2} & W_N^{-4} & \cdots & W_N^{-2(N-1)} \\ \cdots & \cdots & \cdots & \cdots & \cdots \\ 1 & W_N^{-(N-1)} & W_N^{-2(N-1)} & \cdots & W_N^{-(N-1)(N-1)} \end{bmatrix} \tag{13}$$

where $W_N = \exp(j2\pi/N)$.

When the fully polarization is considered, we have

$$\mathbf{e}_{dm} = \mathbf{\Psi}\mathbf{h}_m \tag{14}$$

where $m = 1, 2, 3, 4$ denotes HH, HV, VH and VV channel respectively. $\mathbf{e}_{dm}$ and $\mathbf{h}_m$ denote the fully polarimetric coarse range profiles and HRRPs of full-band OFDM signal respectively.

As analyzed above, via Fourier transform to the received simultaneous fully polarimetric R-OFDM pair echo $y_{\mathrm{H}}(t)$ and $y_{\mathrm{V}}(t)$ given by (8)(9), the coarse range profiles of H and V polarization channel can be obtained, respectively. Then the co-polar and cross-polar parts can get separated by indexing frequencies given by (2)(3). The coarse range profiles of each individual polarization can be regarded to be randomly selected half of that from the full-band OFDM signal. Thus

$$\mathbf{e}_m = \mathbf{\Theta}_m \mathbf{e}_{dm} \tag{15}$$

where $\mathbf{e}_m$ is a $N/2 \times 1$ vector, which denotes the measured coarse range profiles of HH, HV, VH and VV channel obtained by the R-OFDM pair. $\mathbf{\Theta}_m$ is a $N/2 \times N$ sensing matrix. Assuming $\mathbf{I}$ is a $N \times N$ identity matrix, $\mathbf{\Theta}_1 = \mathbf{\Theta}_2 = \mathbf{\Theta}_{\mathrm{H}}$ are constructed by selecting $N/2$ rows from $\mathbf{I}$ according to G_{H} in (2), and $\mathbf{\Theta}_3 = \mathbf{\Theta}_4 = \mathbf{\Theta}_{\mathrm{V}}$ are the rest $N/2$ rows according to G_{V} in (3).

Substitute (14) into (15), then

$$\mathbf{e}_m = \mathbf{\Theta}_m \mathbf{\Psi} \mathbf{h}_m = \mathbf{\Phi}_m \mathbf{h}_m \tag{16}$$

where $\mathbf{\Phi}_m = \mathbf{\Theta}_m \mathbf{\Psi}$ is the mapping matrix.

From (16), $\mathbf{e}_m$ is the sparse coarse range profile obtained from the R-OFDM pair echo, $\mathbf{h}_m$ is the polarimetric HRRPs need to be reconstructed. Assume the target has P scatterers, thus $\mathbf{h}_m$ is P-sparse according to CS theory. Because $\mathbf{\Theta}_m$ is randomly selected from the identity matrix, the restricted isometry property (RIP) condition of the mapping matrix $\mathbf{\Phi}_m$ is satisfied with high probability [20], [21]. Thus the polarimetric HRRPs $\mathbf{h}_m$ can be obtained by solving the following sparse optimization problem

$$\hat{\mathbf{h}}_m = \min ||\mathbf{h}_m||_0 \quad \text{s.t. } ||\mathbf{e}_m - \mathbf{\Phi}_m \mathbf{h}_m||_2 \leq \varepsilon \tag{17}$$

where $||\cdot||_0$ is l_0 norm, $||\cdot||_2$ is l_2 norm,ε is the noise tolerance. For the discontinuity of l_0 norm, l_1 norm usually replaces l_0 norm. Then the optimization model is rewritten as $\hat{\mathbf{h}}_m = \min ||\mathbf{h}_m||_1$. The whole CS-based procedure of polarimetric HRRP reconstruction for each R-OFDM echo can be concluded by Fig.2.

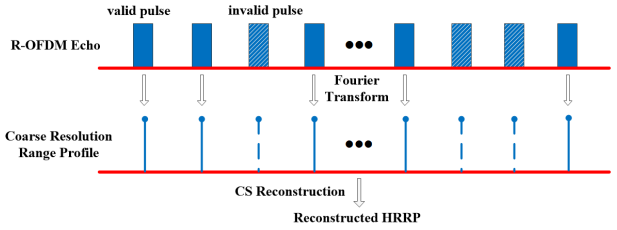

FIGURE 2. CS-based processing procedure of R-OFDM echo.

B. SINGLE POLARIZATION-OMP ALGORITHM

To solve (17), a number of CS reconstruction algorithms are available including basis pursuit(BP), orthogonal matching pursuit (OMP), sparse Bayesian learning(SBL), and so on. In this paper, OMP is selected due to its high efficiency and low time cost [22]. To reconstruct the polarimetric HRRPs, One intuitive method is to directly apply the OMP algorithm to each polarization channel individually, which can be called Single Polarization-OMP (SP-OMP). The detailed algorithm procedure is given as follows.

However, the SP-OMP algorithm may lead to failure in guaranteeing the consistency of the position of the same scatterer in different channels due to the individual processing of different polarization channels. Furthermore, such inconsistency implies that extra scattering center selection and association procedures are needed for further polarimetric analysis.

Algorithm 1 SP-OMP algorithm

Input: measured coarse range profiles $\mathbf{e}_m$, mapping matrixes $\mathbf{\Phi}_m$ and sparsity L.

Output: polarimetric HRRPs $\hat{\mathbf{h}}_m$.

Procedure:

Step 1: Initialize residual vector $\mathbf{r}_0 = \mathbf{e}_m$ and index set $\mathbf{\Lambda}_0 = \emptyset$, set cycle index $l = 0$;

Step 2: Let $l = l + 1$;

Step 3: Find $j = \arg\max| < (\mathbf{\Phi}_m^j)^H, \mathbf{r}_{l-1} > |$, where $< \cdot, \cdot >$ represents correlation coefficients calculation, $\mathbf{\Phi}_m^j$ is the j th column of $\mathbf{\Phi}_m$, $(\cdot)^H$ is conjugate transpose. Then update the index set $\mathbf{\Lambda}_l = \mathbf{\Lambda}_{l-1} \cup \{j\}$;

Step 4: Update sparse solution $\hat{\mathbf{h}}_m$, where positions of non-zero elements are determined by $\mathbf{\Lambda}_l$ with the coefficient $\mathbf{\Gamma}_m = [(\mathbf{\Phi}_{m\Lambda_l})^H \mathbf{\Phi}_{m\Lambda_l}]^{-1} \mathbf{\Phi}_{m\Lambda_l} \mathbf{e}_m$,where $\mathbf{\Phi}_{m\Lambda_l}$ is the matrix constructed by columns of $\mathbf{\Phi}_m$ indexed by $\mathbf{\Lambda}_l$. Update the residual vector $\mathbf{r}_l$, where $\mathbf{r}_l = \mathbf{e}_m - \mathbf{\Phi}_{m\Lambda_l} \mathbf{\Gamma}_m$;

Step 5: If $l > L$, stop the iteration, and output the sparse solution $\hat{\mathbf{h}}_m$; Otherwise back to Step 2.

C. FULLY POLARIZATION-SIMULTANEOUS OMP ALGORITHM

As analyzed in the previous sub-section, the SP-OMP algorithm may lead to the inconsistency of scatterers among different polarization channels due to the individual processing. In fact, scatterers in different polarization channels have the same positions but with different amplitude and phase responses, as revealed in Fig.3. It indicates the fully polarimetric HRRPs are row-sparse [23], [24].

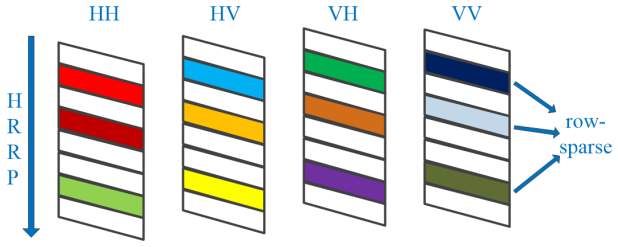

FIGURE 3. Row-sparse model.

The matrix constructed by the fully polarimetric HRRPs is denoted as $\mathbf{H} = [\mathbf{h}_1, \mathbf{h}_2, \mathbf{h}_3, \mathbf{h}_4]$. Similarly, the matrix constructed by the measured coarse range profiles is denoted as $\mathbf{E} = [\mathbf{e}_1, \mathbf{e}_2, \mathbf{e}_3, \mathbf{e}_4]$. The row-sparse optimization model is written as

$$\hat{\mathbf{H}} = \min ||\mathbf{H}||_{row-0} \quad \text{s.t.} \sum_{m=1}^{4} ||\mathbf{e}_m - \mathbf{\Phi}_m \mathbf{h}_m||_2 \leq \varepsilon \tag{18}$$

where $||\cdot||_{row-0} \overset{\text{def}}{=} |\text{rowsupp}(\cdot)|$ is $row - l_0$ norm of the matrix, which represents the number of non-zero rows. Here $||\mathbf{H}||_{row-0} = |||\mathbf{h}_1| + |\mathbf{h}_2| + |\mathbf{h}_3| + |\mathbf{h}_4||_0$.

For row-sparse optimization, [24] proposed a classic greedy algorithm called Simultaneous OMP (SOMP). However, it is applicable only if multiple measurements share the same mapping matrix. However, the mapping matrixes of different polarization channels $\mathbf{\Phi}_m$ in (18) are different according to (16). For the inconsistency of the mapping matrixes, we proposed the reconstruction algorithm called Fully Polarization-SOMP (FP-SOMP) by improving the SOMP algorithm, which is listed as follows.

Algorithm 2 FP-SOMP algorithm

Input: matrix of the measured coarse range profiles $\mathbf{E}$, mapping matrixes $\mathbf{\Phi}_m$ and row-sparsity L.

Output: polarimetric HRRPs $\widehat{\mathbf{H}}$.

Procedure:

Step 1: Initialize residual matrix $\mathbf{R_0} = \mathbf{E}$ and index set $\mathbf{\Lambda}_0 = \emptyset$, set cycle index $l = 0$;

Step 2: Let $l = l + 1$;

Step 3: Find $j = \arg\max \sum_{m=1}^{4} | < (\mathbf{\Phi}_m^j)^H, \mathbf{R}_{l-1}^m > |$, where $\mathbf{R}_{l-1}^m$ is the m th column of $\mathbf{R}_{l-1}$. Then update index set $\mathbf{\Lambda}_l = \mathbf{\Lambda}_{l-1} \cup \{j\}$;

Step 4: Update the sparse solution $\widehat{\mathbf{H}}$, where the positions of nonzero elements are determined by $\mathbf{\Lambda}_l$. For mth polarization channel, the coefficient of non-zero elements is $\mathbf{\Gamma}_m = [(\mathbf{\Phi}_{m\Lambda_l})^H \mathbf{\Phi}_{m\Lambda_l}]^{-1} \mathbf{\Phi}_{m\Lambda_l} \mathbf{E}_m$,where $\mathbf{E}_m$ is mth column of $\mathbf{E}$. Update the residual matrix $\mathbf{R}_l$, where $\mathbf{R}_l^m = \mathbf{E}_m - \mathbf{\Phi}_{m\Lambda_l} \mathbf{\Gamma_m}$;

Step 5: If $l > L$, stop the iteration, and output the sparse solution $\widehat{\mathbf{H}}$; Otherwise back to Step 2.

Compared with SP-OMP, the proposed FP-SOMP algorithm processes all the polarization channels and outputs the reconstructed polarimetric HRRPs simultaneously. Hence the consistency of the scatterers among different polarization channels is guaranteed. Besides, the accuracy of the reconstructed polarimetric HRRPs can be improved due to the joint information utilization.

The procedure of the R-OFDM pair and FP-SOMP reconstruction algorithm is concluded in Fig.4.

Each of the received R-OFDM pair echo, $y_{\mathrm{H}}(t)$ and $y_{\mathrm{V}}(t)$ from two orthogonal polarizations includes both co-polar and cross-polar information. The signals from the two receiving channels are each processed in two branches.

Firstly, Fourier transform (FT) is executed for time-frequency transform and the outputs are denoted as $e_{\mathrm{H}}(i)$ and $e_{\mathrm{V}}(i)$ respectively.

Next, the discrete sequence in frequency domain is selected at the frequency point $f_{\mathrm{H}n}$ and $f_{\mathrm{V}n}$, respectively. Then the co-polar and cross-polar parts get separated. The coarse range profiles of the all four polarization channels $e_{\mathrm{HH}}(i)$, $e_{\mathrm{HV}}(i)$,$e_{\mathrm{VH}}(i)$ and $e_{\mathrm{VV}}(i)$ are obtained.

Finally, The polarimetric HRRPs $\hat{h}_{\mathrm{HH}}(k)$,$\hat{h}_{\mathrm{HV}}(k)$,$\hat{h}_{\mathrm{VH}}(k)$ and $\hat{h}_{\mathrm{VV}}(k)$ are obtained by the proposed FP-SOMP reconstruction.

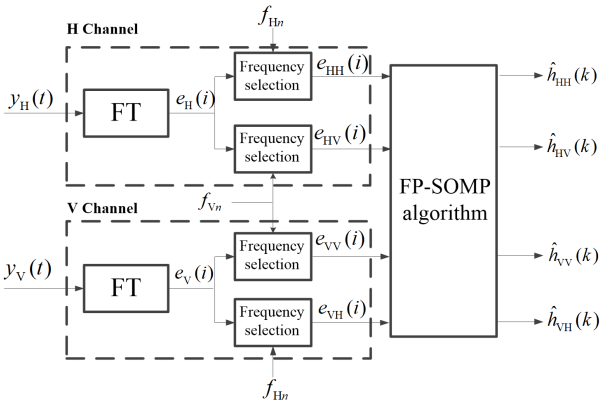

FIGURE 4. The signal processing procedure.

TABLE 1. Parameters of the full-band OFDM signal.

carrier frequency (f_0)	10GHz	bandwidth (B)	600MHz
sub-pulse number (N)	200	sub-pulse width (τ)	0.5us
frequency interval (Δf)	3MHz	PRI (T)	1us

TABLE 2. PSM of the scatterers.

serial number	span{**S**}	S_{HH}	S_{HV}	S_{VH}	S_{VV}
1	0.9487	0.6	0.3	0.3	0.6
2	0.7937	0.5	0.1	0.1	0.6
3	1.000	0.5	0.5	0.5	0.5
4	1.416	1	0.05	0.05	1

IV. NUMERICAL SIMULATION

A. SIMULATION DESCRIPTIONS

In this section, the numerical simulation is conducted to demonstrate the validity of the proposed simultaneous polarimetric HRRP renconstruction method. Assume an X-band radar operating at 10GHz, the parameters of the full-band OFDM signal are listed in Table 1. According to the signal parameters, the unambiguous range is $\Delta r = [-c/4\Delta f, c/4\Delta f] = [-25\mathrm{m}, 25\mathrm{m}]$. The target is formed of four scatterers, then the sparsity is $L = 4$. The distance between the scatterers and reference point is $R = [-5\mathrm{m}, 8\mathrm{m}, 10\mathrm{m}, 14\mathrm{m}]$, and the PSMs of scatterers are listed in Table 2.

Firstly, if the I-OFDM pair proposed in [11] is applied by alternately selecting the sub-pulses from the full-band OFDM signal, Fig.5 presents the polarimetric HRRPs with the DFT-based processing algorithm, where the blue dashed lines represent the obtained polarimetric HRRPs, and the red lines marked by '$\times$' represent the correct positions of the scatterers. As shown in Fig.5, the unambiguous range for I-OFDM pair is $[-12.5\mathrm{m}, 12.5\mathrm{m}]$, thus a fake peak appears at $-11\mathrm{m}$ for Scatterer 4. Hence the HRRPs are coupled in the range direction, which indicates the failure of polarimetric HRRP reconstruction.

B. PERFORMANCE ANALYSES OF THE R-OFDM PAIR

Randomly select half of the sub-pulses (i.e.100 sub-pulses) from the full-band OFDM signal as the H channel signal,

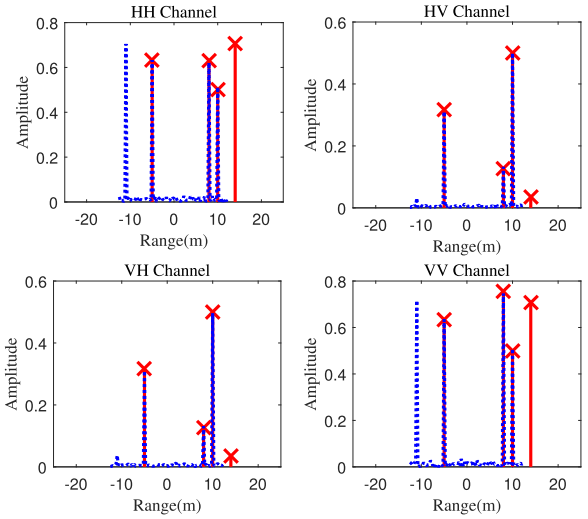

FIGURE 5. Performance of I-OFDM pair.

and the rest half as the V channel signal, then the proposed R-OFDM pair is obtained. The performance of the proposed R-OFDM pair with two CS-based algorithms in Section III is presented from the following three aspects: reconstrction probability of polarimetric HRRPs, mean square error (MSE) of PSM estimation and influence of sparsity settings.

1) RECONSTRUCTION PROBABILITY IN THE PRESENCE OF NOISE

Firstly, the reconstruction probability of CS-based algorithms in the presence of noise is presented. From the algorithm procedure, the sparsity is the core input parameter, which should be equal to the number of scatterers according to CS theory. Here assume the sparsity is known as a prior information. Then we have $L = 4$.

Fig.6 presents the reconstructed polarimetric HRRPs with the signal-to-noise ratio (SNR) set as 20dB and 10dB respectively, where the blue lines marked by '□' represent the HRRPs reconstructed by SP-OMP, the black lines marked by 'Δ' represent the HRRPs reconstructed by FP-SOMP.

Firstly, when comparing the obtained polarimetric HRRPs in Fig.6 with that of I-OFDM pair in Fig.5, it is shown that all scatterers including Scatterer 4 (as marked by the arrows in Fig.6) can be successfully reconstructed when the proposed R-OFDM pair is adopted. It is because the unambiguous range is $[-25\text{m}, 25\text{m}]$ for R-OFDM pair, which is the same as the full-band OFDM signal. Then a wider unambiguous range is obtained, and the polarimetric HRRPs are not coupled, which is in accordance with theoretical analyses. Hence the superiority of the proposed R-OFDM pair is demonstrated.

Next, when comparing the two CS-based algorithms for R-OFDM pair, both algorithms reconstruct the polarimetric HRRPs successfully when SNR $=$ 20dB as shown in Fig.6(a). However, when SNR decreases to 10dB, the SP-OMP algorithm fails to reconstruct the weak scatterers of HV and VH channel, whereas the proposed FP-SOMP is still effective for polarimetric HRRP reconstruction,as shown in Fig.6(b).

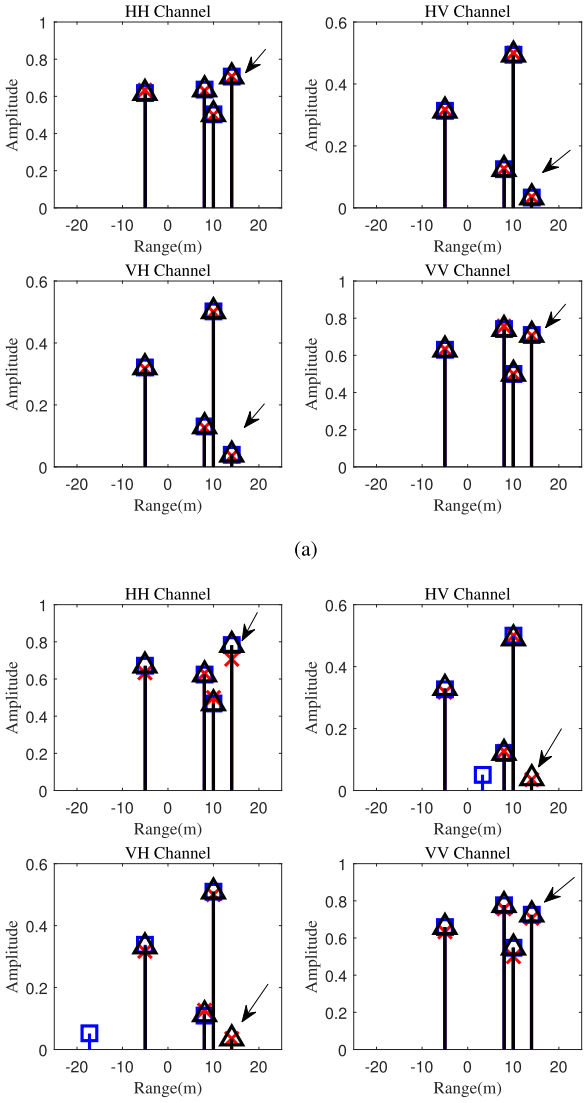

FIGURE 6. Reconstructed polarimetric HRRPs in the presence of noise. (a). SNR = 20dB. (b) SNR = 10dB.

Further, assume SNR varies from -20dB to 20dB stepped by 1dB, and 1000 Monte-Carlo simulations are conducted for each SNR. The reconstruction probability of each polarization channel and the overall reconstruction probability are presented in Fig.7. It is necessary to point out that a successful reconstruction means that the positions of all scatterers are correctly reconstructed here.

As shown in Fig.7(a), for both SP-OMP and FP-SOMP, the polarimetric HRRPs cannot be reconstructed when SNR is lower than -11dB whereas can be precisely obtained when SNR is higher than 17dB. When SNR is among -11dB to 17dB, the reconstruction probabilities of the co-polar channel are higher than the cross-polar channel for SP-OMP. It is reasonable considering the stronger scattering intensity in

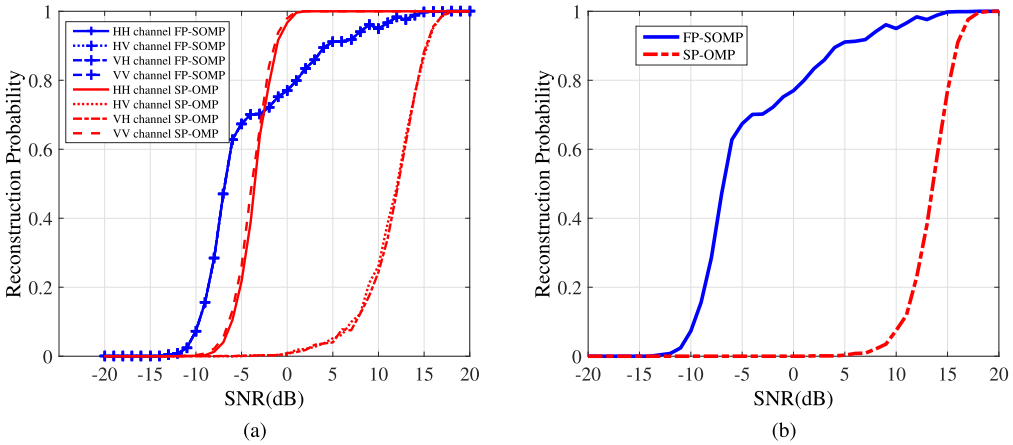

FIGURE 7. Reconstruction probability in the presence of noise. (a). Reconstruction probability of each individual channel. (b). Overall reconstruction probability.

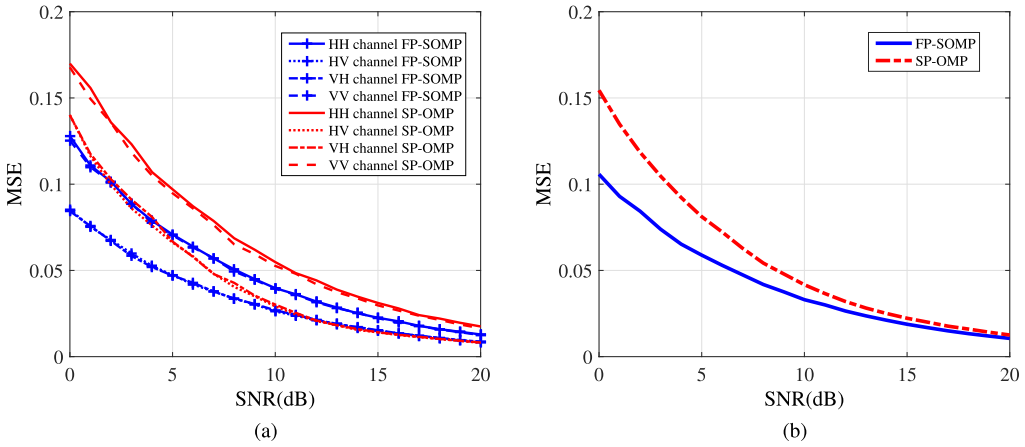

FIGURE 8. MSE of PSM estimation. (a). MSE of each polarization channel. (b). Average MSE.

co-polar channel. While the reconstruction probability of different polarization channels is the same due to the joint processing for FP-SOMP. As shown in Fig.7(b), the overall reconstruction probability of FP-SOMP is much higher than SP-OMP, which is in accordance with the theoretical analysis. Hence FP-SOMP is more efficient than SP-OMP, especially in low SNRs. Specially, to gain the reconstruction probability no less than 0.8, the required SNR is 1dB for FP-SOMP and 15dB for SP-OMP respectively. To gain the reconstruction probability no less than 0.9, the required SNR is 5dB for FP-SOMP and 17dB for SP-OMP respectively.

2) MSE OF PSM ESTIMATION

In this sub-section, the MSE of PSM estimation is further analyzed to evaluate the accuracy of reconstructed scatterering amplitude, which is given in Fig.8. As shown in Fig.8(a), when SNR increases, MSE of PSM estimation rapidly reduces for all polarization channels. MSE of co-polar channels is higher than that of the cross-polar channels for both methods. Besides, the MSE for FP-SOMP is smaller than that for SP-OMP, as revealed in Fig.8(b). Specially, to gain the satisfying PSM estimations, a SNR no less than 1dB(MSE $<$ 0.1) and 7dB(MSE $<$ 0.05)is required for FP-SOMP. However, the threshold increases to 4dB(MSE $<$ 0.1) and 9dB(MSE $<$ 0.05) for SP-OMP. It can be concluded that more accurate polarimetric HRRPs can be obtained by the FP-SOMP algorithm.

3) INFLUENCE OF SPARSITY SETTINGS

As analyzed above, the sparsity is an important input parameter for both CS-based algorithms. In previous simulations, the sparsity is simply assumed as a prior information. However,the sparsity is usually unknown in actual applications, especially for the targets with complex structures. In this subsection, the influence of sparsity settings is analyzed. Fig.9(a) and (b) present the reconstructed polarimetric HRRPs with the sparsity set as $L = 5$ and $L = 10$ respectively, where SNR $=$ 20dB.

As shown in Fig.9, when SP-OMP is applied, more and more fake scatterers appear with the increase of sparsity

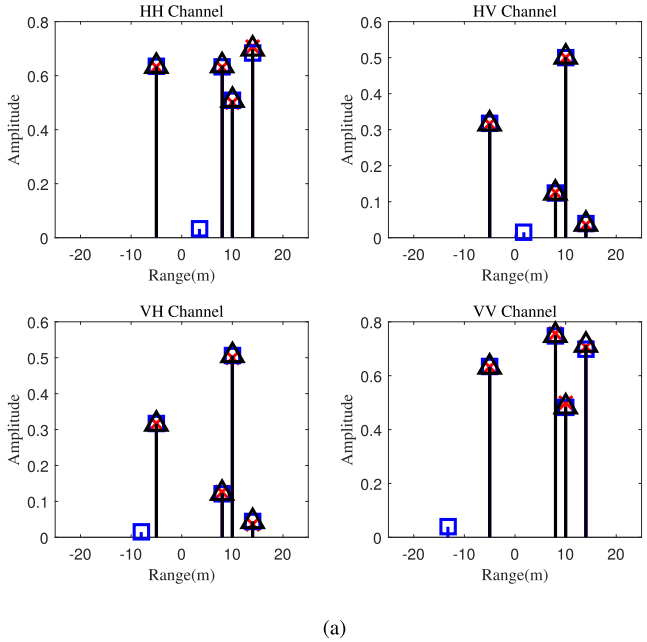

(a)

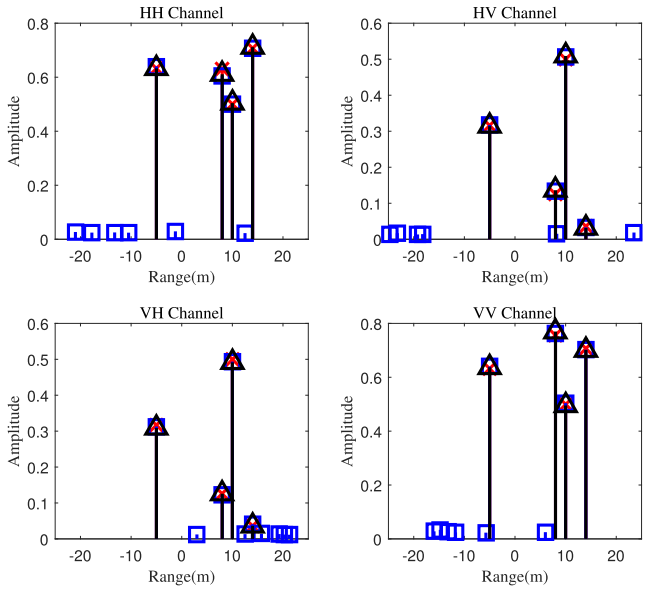

(b)

FIGURE 9. Reconstructed polarimetric HRRPs with different sparsity settings. (a) $L = 5$. (b). $L = 10$.

mismatch. The appearance of fake scatterers increases the difficulty of scattering center selection and association. However, when FP-SOMP is applied, the polarietric HRRPs can still be successfully reconstructed even if the sparsity is set as $L = 10$. It means the accurate number of scatterers is not the essential prior information for the proposed FP-SOMP algorithm. A larger sparsity can be set by experience, which reduces the dependence on the prior information in actual applications. Hence it can be concluded that a more robust HRRP reconstruction performance can be obtained by the proposed FP-SOMP algorithm.

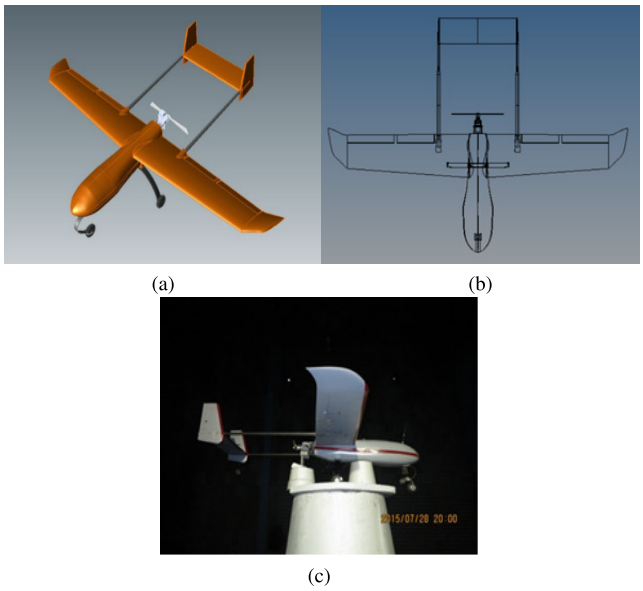

(a) (b)

(c)

FIGURE 10. The "FRONTIER" UAV model. (a).General shape. (b). Front view. (c). Model in the microwave anechoic chamber scene.

From the numerical simulation, the following conclusions can be made.

1) Compared with I-OFDM pair, a wider unambiguous range can be obtained by the proposed R-OFDM pair signal, hence the polarimetric HRRPs of the large-size target will not be coupled.
2) The CS-based algorithms are qualified to reconstruct the polarimetric HRRPs for the R-OFDM pair, hence the validity of the proposed method is demonstrated. Besides, by exploiting the joint sparsity of different polarization channels, a better polarimetric HRRP reconstruction performance can be obtained with the proposed FP-SOMP algorithm compared with the SP-OMP algorithm.

V. VERIFICATIONS WITH MEASURED UAV DATA

In this section, measured data simulations are further conducted to verify the validity of the proposed method. The unmanned aerial vehicle(UAV) data obtained by electromagnetic calculations and microwave anechoic chamber measurements are separately used for the verifications.

A. POLARIMETRIC UAV DATA WITH THE FULL-BAND OFDM SIGNAL

The "FRONTIER" UAV model used for the simulation is shown in Fig.10. The length is 2.3m, the wingspan is 2.9m and the height is 0.66m. As shown in Fig.10(b), the nose is placed along the X axis, which is defined as the 0° of azimuth direction.

The polarimetric UAV datasets with the full-band OFDM signal are firstly obtained. The parameters of OFDM signal are listed in Table 3. As shown in Table 3, the full-band OFDM signal is formed of 200 sub-pulses with the

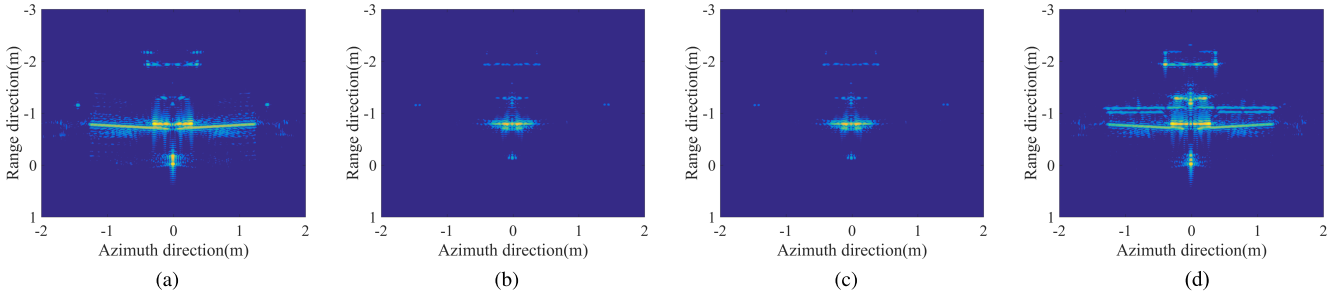

FIGURE 11. 2D UAV image by electromagnetic calculations. (a). HH channel. (b). HV channel. (c). VH channel. (d). VV channel.

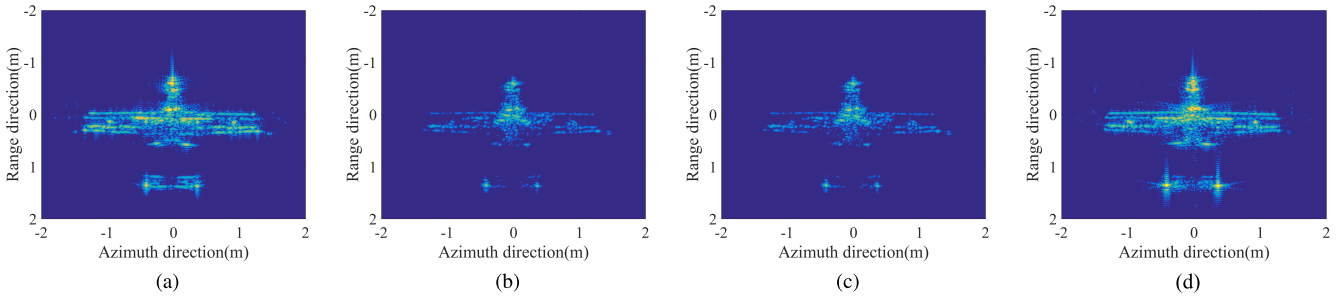

FIGURE 12. 2D UAV image by microwave anechoic chamber measurements. (a). HH channel. (b). HV channel. (c). VH channel. (d). VV channel.

TABLE 3. Signal parameters of the full-band OFDM signal.

start frequency	8GHz	bandwidth	4GHz
stop frequency	12GHz	elevation angle	0°
frequency interval	20MHz	azimuth angle	$-180° \sim 180°$
frequency number	200	azimuth interval	0.2°

frequency ranging from 8GHz to 12GHz, and the bandwidth is 4GHz. The elevation angle is 0°, and the fully polarimetric data of azimuth angle from $-180°$ to 180° with 0.2° interval are recorded. On the one hand, electromagnetic calculations with the all-metal model are executed by FEKO. On the other hand, the measurements with the real UAV model are conducted in the microwave anechoic chamber. The scene is shown in Fig.10(c). Different from the all-metal model in the electromagnetic calculations, the UAV model in the microwave anechoic chamber measurements is made up of various materials including glass fiber reinforced plastics(GFRP), carbon fiber, wood and metal. The swept-frequency signal generated by the vector network analyzer(VNA) is used in the measurements. Since the swept-frequency signal is also formed by sub-pulses with stepped frequencies, it is equivalent with the full-band OFDM signal in the experiment.

Fig.11 and Fig.12 present the two dimensional (2D) polarimetric images with the UAV data obtained by electromagnetic calculations and microwave anechoic chamber measurements respectively, where the azimuth angle varies from $-5°$ to 5°. As shown in Fig.11 and Fig.12, the polarimetric images are in accordance with the UAV model including the shape and size. Hence both of the acquired data are demonstrated to be valid for simulation conduction. Besides, it is obvious that the images of the two datasets are somewhat different, which is reasonable considering the material difference between two models. Due to the difference, both of them are utilized to demonstrate the validity of the proposed method more adequately. For convenience, denote the data of electromagnetic calculations as DATASET 1, and the data of microwave anechoic chamber measurements as DATASET 2.

B. PERFORMANCE OF THE R-OFDM PAIR

Firstly, to obtain the proposed R-OFDM pair signal, randomly select half of the sub-pulses from the full-band OFDM signal as the H channel signal, and the rest as the V channel signal. By indexing the relevant segments of UAV datasets with full-band OFDM signal according to frequency, the polarimetric R-OFDM data for each channel can be simulated. In the simulation, the data at azimuth direction 0° of both datasets are selected for polarimetric HRRP reconstruction. It is necessary to point out that the ideal polarimetric HRRPs are unknown due to the complex scattering property of the UAV model. Via FFT transform, the polarimetric HRRPs with full-band OFDM signal are obtained, and it is treated as the actual HRRPs of the UAV model approximately. Then the HRRPs obtained by the proposed R-OFDM pair can

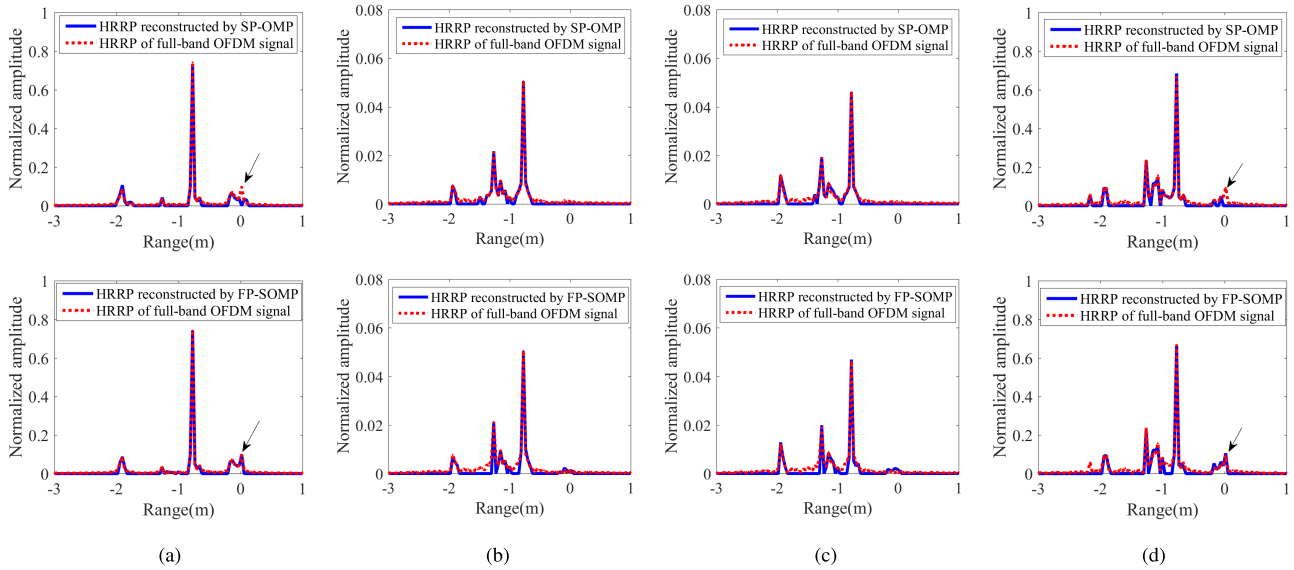

FIGURE 13. Reconstructed polarimetric HRRPs with $L = 20$ (DATASET 1). (a). HH channel. (b). HV channel. (c). VH channel. (d). VV channel.

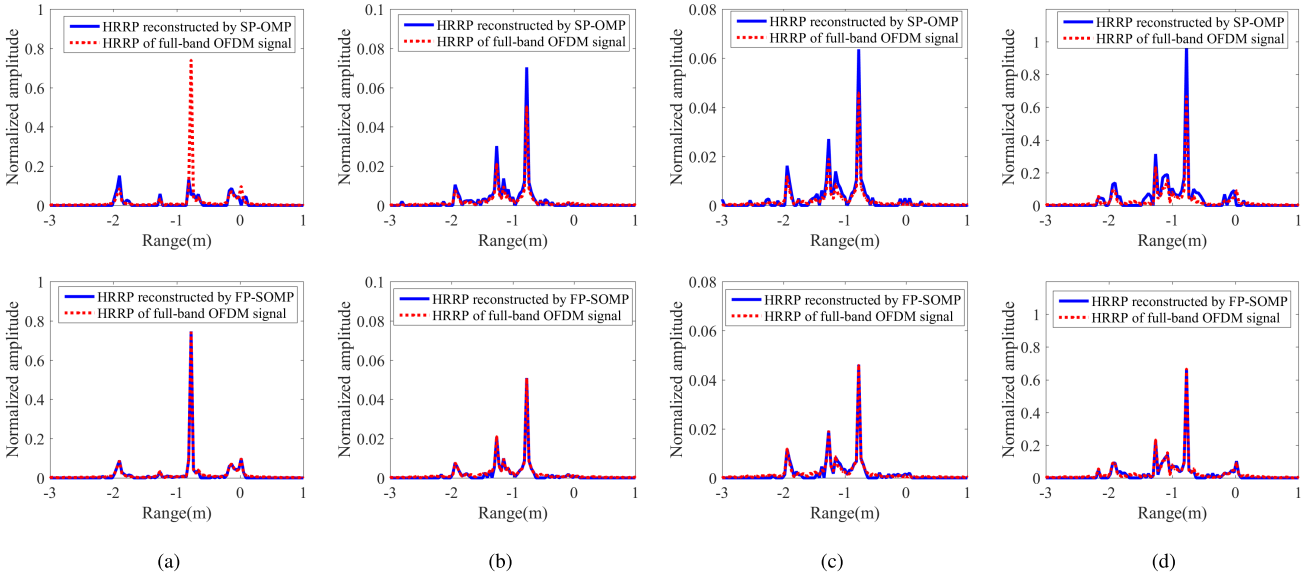

FIGURE 14. Reconstructed polarimetric HRRPs with $L = 40$ (DATASET 1). (a). HH channel. (b). HV channel. (c). VH channel. (d). VV channel.

get quantitatively evaluated by comparison with that obtained by the full-band OFDM signal.

1) COMPARISON OF THE RECONSTRUCTED POLARIMETRIC HRRPS

For the proposed R-OFDM pair, the polarimetric HRRPs can be reconstructed by applying the CS-based SP-OMP and FP-SOMP algorithms respectively. Due to the complex scattering property of the UAV model, the sparsity remains unknown for the reconstruction algorithm. Fig.13 to Fig.16 present the reconstructed polarimetric HRRPs with different sparsities, where it is set as $L = 20$ and $L = 40$ for DATASET 1 and $L = 40$ and $L = 60$ for DATASET 2, respectively. The sparsity of DATASET 2 is set a bit larger than that of DATASET 1 due to the more complex scattering property of various material structures of the UAV model in anechoic chamber measurements.

As shown in Fig.13 and Fig.15, when the sparsity is set as $L = 20$ for DATASET 1 and $L = 40$ for DATASET 2, both of the algorithms can reconstruct the polarimetric HRRPs correctly. Hence it is demonstrated that the R-OFDM pair and the CS-based algorithm are qualified for polarimetric HRRP reconstruction. Besides, the weak scatterers in the HRRPs can be reconstructed more accurately by the FP-SOMP

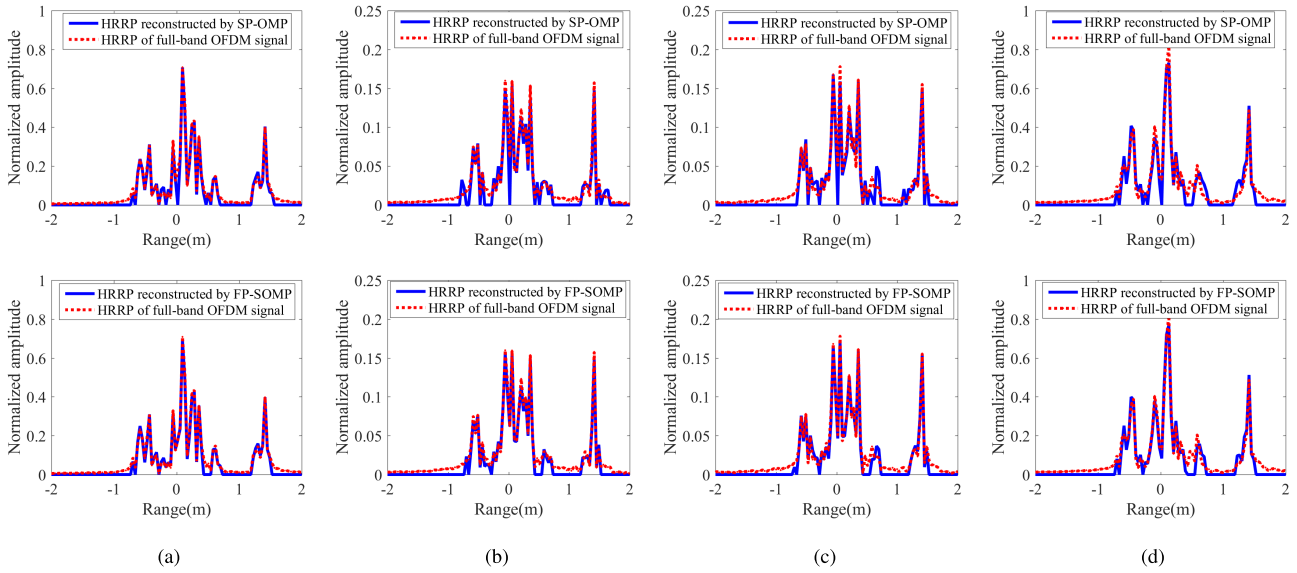

FIGURE 15. Reconstructed polarimetric HRRPs with $L = 40$ (DATASET 2). (a). HH channel. (b). HV channel. (c). VH channel. (d). VV channel.

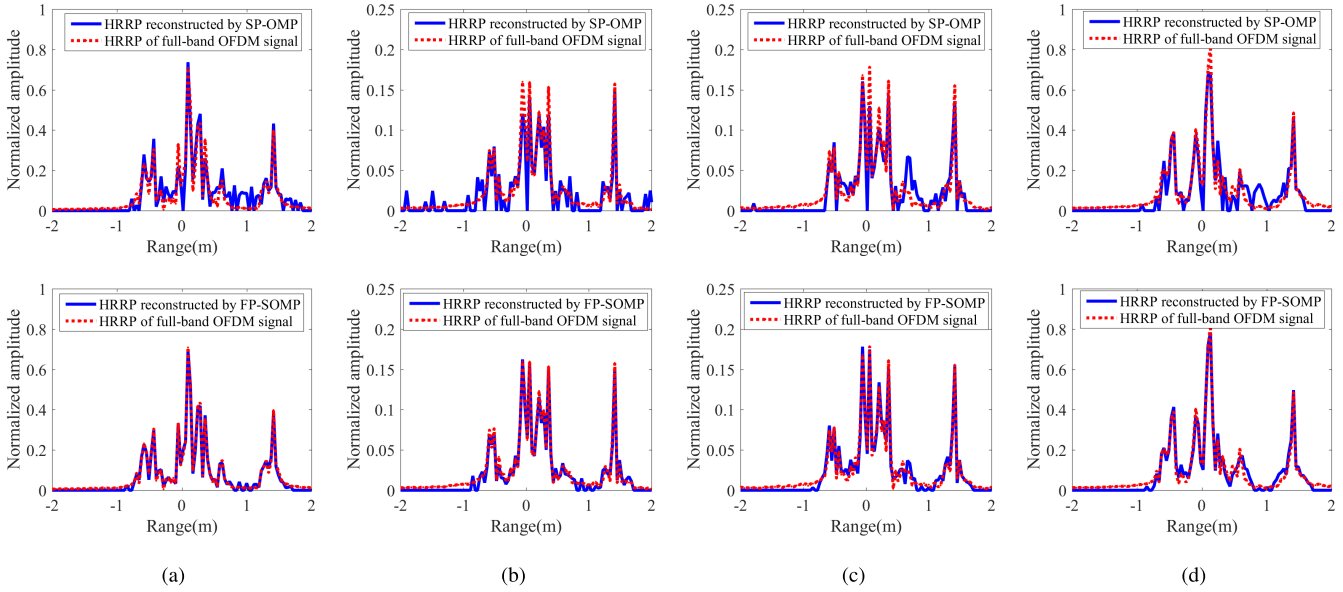

FIGURE 16. Reconstructed polarimetric HRRPs with $L = 60$ (DATASET 2). (a). HH channel. (b). HV channel. (c). VH channel. (d). VV channel.

algorithm compared with the SP-OMP algorithm due to the joint processing, e.g. the parts marked by arrows in Fig.13(a) and Fig.13(d).

As revealed in Fig.14 and Fig.16, when the sparsity increases to $L = 40$ for DATASET 1 and $L = 60$ for DATASET 2, the SP-OMP algorithm totally fails to reconstruct the polarimetric HRRPs, whereas the proposed FP-SOMP algorithm can still reconstruct the HRRPs correctly. Hence it can be concluded that the FP-SOMP algorithm is more robust than SP-OMP algorithm.

2) EVALUATION OF THE POLARIMETRIC HRRP RECONSTRUCTION PERFORMANCE

Due to the complex scattering properties of the UAV model, the PSM of the scatterers cannot be calculated. To quantificationally evaluate the polarimetric HRRP reconstruction performance of the proposed CS-based algorithm, a novel indicator called degree of distortion γ can be defined as

$$\gamma = \sum_{j=1}^{N} \left| |h_r(j)| - |h_f(j)| \right| / \sum_{j=1}^{N} |h_f(j)| \tag{19}$$

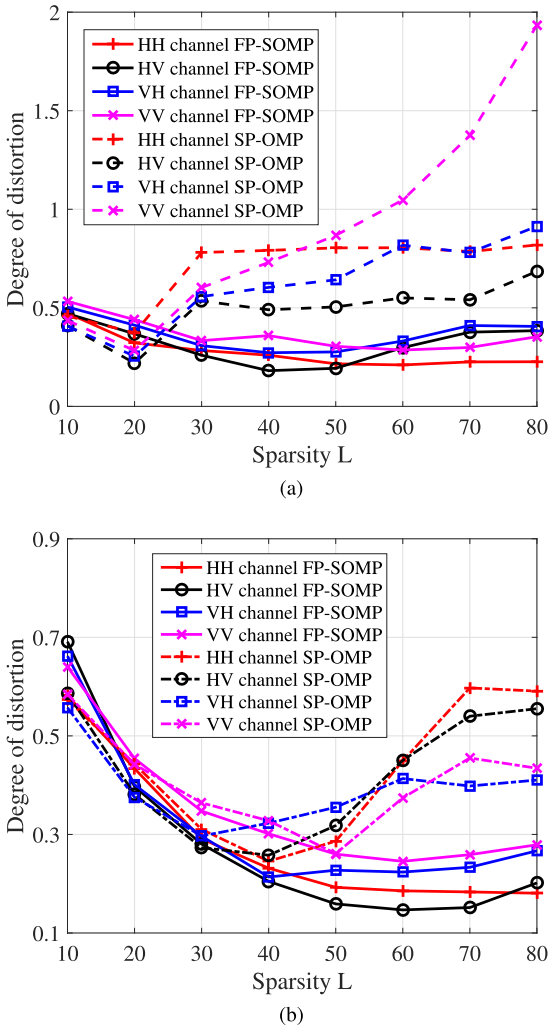

FIGURE 17. Degree of distortion with the sparsity varying from 10 to 80. (a) DATASET 1. (b). DATASET 2.

where h_r is the reconstructed HRRP sequence, h_f is the ideal HRRP sequence, N is the length of the HRRP sequence. It is obvious that the smaller the degree of distortion γ, the better the HRRP reconstruction performance. When $\gamma = 0$, the ideal reconstruction performance is obtained. However, the ideal polarimetric HRRPs of the UAV are unknown as analyzed above. Hence the polarimetric HRRPs of the full-band OFDM signal are used as the actual HRRPs approximatively. It is necessary to point out that the calculated degree of distortion may be a little larger than 0 even if the polarimetric HRRPs are ideally reconstructed due to this equivalence. Fig.17 presents the degree of distortion when the sparsity varies from 10 to 80 with 10 stepping for DATASET 1 and DATASET 2.

As revealed in Fig.17, when the SP-OMP algorithm is applied, the degree of distortion firstly drops then rapidly grows with the increase of the sparsity. It is because the sparsity L should be equal to the number of scatterers according to CS theory. When L is smaller the number of scatterers, some real scatterers are not reconstructed. Whereas L is larger than the number of scatterers, some fake scatterers will appear. Specially, when $L = 20$ for DATASET 1 and $L = 40$ for DATASET 2, the minimum degree of distortion (also the best reconstructed HRRPs) can be obtained. However, it is not practical to always obtain the accurate sparsity in actual applications.

When the proposed FP-SOMP algorithm is applied, the degree of distortion greatly reduces compared with the SP-OMP algorithm due to the joint processing, which indicates that the polarimetric HRRPs are reconstructed more accurately. Besides, the degree of distortion keeps relatively stable with the increase of sparsity when the threshold is satisfied (i.e. $L = 20$ for DATASET 1 and $L = 40$ for DATASET 2). It indicates that a more robust HRRP reconstruction performance can be obtained by releasing the dependence on the accurate sparsity settings in actual applications. The results are in accordance with the polarimetric HRRPs given by Fig.13 to Fig.16 and the conclusions given by numerical simulations in Section IV.

In conclusion, the UAV data experiments indicate that the R-OFDM pair and the CS-based algorithm are qualified for polarimetric HRRP reconstruction. Besides, a more robust reconstruction performance can be obtained by the proposed FP-SOMP algorithm compared with the SP-OMP algorithm.

VI. CONCLUSION

In this paper, a novel R-OFDM pair is proposed for simultaneous polarimetric HRRP reconstruction. By joint processing of different polarization channels, the CS-based algorithm called FP-SOMP is proposed instead of SP-OMP algorithm. Then the polarimetric HRRPs are reconstructed more accurately and robustly. Both numerical simulations and UAV data experiments indicate that the combination of R-OFDM pair and the CS-based FP-SOMP algorithm is an efficient trail for simultaneous polarimetric HRRP reconstruction. In future, further analyses focusing on its application in 2D radar imaging such as polarimetric synthetic aperture radar(polSAR) and inverse SAR (polISAR) will be conducted. Besides, the random selection theory also has the potential in the application of some other types of signals such as SFW and LFM. Further work on this topic will be beneficial to enrich the related knowledge.

REFERENCES

[1] Q. Song, F. Xu, and Y. Jin, "Radar image colorization: Converting single-polarization to fully polarimetric using deep neural networks," *IEEE Access*, vol. 6, pp. 1647–1661, 2018.
[2] S. Zhang, B. Hou, L. Jiao, Q. Wu, C. Sun, and W. Xie, "Context-based max-margin for PolSAR image classification," *IEEE Access*, vol. 5, pp. 24070–24077, 2017.
[3] A. Y. Nashashibi, K. Sarabandi, P. Frantzis, R. D. De Roo, and F. T. Ulaby, "An ultrafast wide-band millimeter-wave (MMW) polarimetric radar for remote sensing applications," *IEEE Trans. Geosci. Remote Sens.*, vol. 40, no. 8, pp. 1777–1786, Aug. 2002.
[4] J. Dall *et al.*, "ESA'S POLarimetric airborne radar ice sounder (POLARIS): Design and first results," *IET Radar Sonar Navigat.*, vol. 4, no. 3, pp. 488–496, 2010.
[5] D. Giul, "Polarization diversity in radars," *IEEE Proc.*, vol. 74, no. 2, pp. 245–269, Feb. 1986.
[6] D. Giul, L. Facheris, M. Fossi, and A. Rossettini, "Simultaneous scattering matrix measurement through signal coding," in *Proc. IEEE Int. Radar Conf.*, Arlington, VA, USA, May 1990, pp. 258–262.

[7] D. Giul, M. Fossi, and L. Facheris, "Radar target scattering matrix measurement through orthogonal signals," *IEE Proc. F-Radar Signal Process.*, vol. 140, no. 4, pp. 233–242, Aug. 1993.
[8] R. van Nee and R. Prasad, *OFDM for Wireless Multimedia Communications*. Norwood, MA, USA: Artech House, 2000.
[9] W. Cao, X. Li, H. Wei-Dong, J. Lei, and W. Zhang, "OFDM Reference signal reconstruction exploiting subcarrier-grouping based multi-level lloyd-max algorithm in passive radar systems," *IET Radar Sonar Navigat.*, vol. 11, no. 5, pp. 873–879, 2016.
[10] G. Lellouch, A. Mishra, and M. Inggs, "Orthogonal frequency division multiplexing phenomenology: Radar technique combining genetic algorithm-based pulse design and energy detector for target recognition," *IET Radar Sonar Navigat.*, vol. 10, no. 5, pp. 912–922, 2016.
[11] Z. Wang, F. Tigrek, O. Krasnov, F. Van Der Zwan, P. Van Genderen, and A. Yarovoy, "Interleaved OFDM radar signals for simultaneous polarimetric measurements," *IEEE Trans. Aerospace Electron. Syst.*, vol. 48, no. 3, pp. 2085–2099, Jul. 2012.
[12] Y. Luo, Q. Zhang, W. Hong, and Y. Wu, "Waveform design and high-resolution imaging of cognitive radar based on compressive sensing," *Sci. China Inf. Sci.*, vol. 55, no. 11, pp. 2590–2603, 2012.
[13] H. Li, Y. Zhao, Z. Cheng, and D.-Z. Feng, "Orthogonal frequency division multiplexing linear frequency modulation signal design with optimised pulse compression property of spatial synthesised signals," *IET Radar Sonar Navigat.*, vol. 10, no. 7, pp. 1319–1326, 2016.
[14] D. L. Donoho, "Compressed sensing," *IEEE Trans. Inf. Theory*, vol. 52, no. 4, pp. 1289–1306, Apr. 2006.
[15] A. N. O'Donnell, J. L. Wilson, D. M. Koltenuk, and R. J. Burkholder, "Compressed sensing for radar signature analysis," *IEEE Trans. Aerosp. Electron. Syst.*, vol. 49, no. 4, pp. 2631–2639, Oct. 2013.
[16] A. Bacci, D. Staglianò, E. Giusti, S. Tomei, F. Berizzi, and M. Martorella, "Compressive sensing for interferometric inverse synthetic aperture radar applications," *IET Radar Sonar Navigat.*, vol. 10, no. 8, pp. 1446–1457, Oct. 2016.
[17] L. Zhang, B. Li, N. Xie, and H. Wang, "CSVE radar: High-range-resolution radar using compressive sensing and virtual expanding technique," *IET Radar Sonar Navigat.*, vol. 11, no. 6, pp. 1002–1010, Jun. 2017.
[18] L. Zhang, Z.-J. Qiao, M. Xing, Y. Li, and Z. Bao, "High-resolution ISAR imaging with sparse stepped-frequency waveforms," *IEEE Trans. Geosci. Remote Sens.*, vol. 49, no. 11, pp. 4630–4651, Nov. 2011.
[19] Y. Luo, Q. Zhang, C.-W. Qiu, X.-J. Liang, and K.-M. Li, "Micro-Doppler effect analysis and feature extraction in ISAR imaging with stepped-frequency chirp signals," *IEEE Trans. Geosci. Remote Sens.*, vol. 48, no. 4, pp. 2087–2098, 2010.
[20] Y. Meyer, "The restricted isometry property and its implications for compressed sensing," *Comp. Rendus Mathematique*, vol. 346, nos. 9–10, pp. 589–592, 2008.
[21] E. Candès, J. Romberg, and T. Tao, "Stable signal recovery from incomplete and inaccurate measurements," *Commun. Pure Appl. Math.*, vol. 59, no. 8, pp. 1207–1223, 2006.
[22] J. A. Tropp and A. C. Gilbert, "Signal recovery from random measurements via orthogonal matching pursuit," *IEEE Trans. Inf. Theory*, vol. 53, no. 12, pp. 4655–4666, Dec. 2007.
[23] W. Qiu, H. Zhao, J. Zhou, and Q. Fu, "High-resolution fully polarimetric ISAR imaging based on compressive sensing," *IEEE Trans. Geosci. Remote Sens.*, vol. 52, no. 10, pp. 6119–6131, Oct. 2014.
[24] J. A. Tropp, A. C. Gilbert, and M. J. Strauss, "Algorithms for simultaneous sparse approximation. Part I: Greedy pursuit," *Signal Process.*, vol. 86, no. 3, pp. 572–588, 2006.
[25] J.-F. Determe, J. Louveaux, L. Jacques, and F. Horlin, "On the noise robustness of simultaneous orthogonal matching pursuit," *IEEE Trans. Signal Process.*, vol. 65, no. 4, pp. 864–875, Feb. 2017.
[26] B. Xu, Y. Cui, B. Zuo, J. Yang, and J. Song, "Polarimetric SAR image filtering based on patch ordering and simultaneous sparse coding," *IEEE Trans. Geosci. Remote Sens.*, vol. 54, no. 7, pp. 4079–4093, Jul. 2016.
[27] D. Kim and J. Haldar, "Greedy algorithms for nonnegativity-constrained simultaneous sparse recovery," *Signal Process.*, vol. 125, pp. 274–289, Aug. 2016.
[28] W. Chen, D. Wipf, Y. Wang, Y. Liu, and I. J. Wassell, "Simultaneous Bayesian sparse approximation with structured sparse models," *IEEE Trans. Signal Process.*, vol. 64, no. 23, pp. 6145–6159, Dec. 2016.
[29] P. Babu and P. Stoica, "Spectral analysis of nonuniformly sampled data—A review," *Digit. Signal Process.*, vol. 20, no. 2, pp. 359–378, 2010.
[30] M. I. Skolnik, *Introduction to Radar Systems*. Boston, MA, USA: McGraw-Hill, 2001.

QIHUA WU was born in Yancheng, Jiangsu, China, in 1990. He received the B.S. degree in communication engineering from Nanjing University, Nanjing, China, in 2013, and the M.S. degree in information and communication engineering from the National University of Defense Technology, Changsha, China, in 2015, where he is currently pursuing the Ph.D. degree with the State Key Laboratory of Complex Electromagnetic Environmental Effects on Electronics and Information System.

His research interests include radar imaging techniques and radar signal processing.

FENG ZHAO was born in Nanjing, Jiangsu, China, in 1978. He received the B.S. degree in electronic engineering and the Ph.D. degree in information and communication engineering from the NUDT, Changsha, China, in 2001 and 2007, respectively.

He is currently an Associate Professor with NUDT. His research interests include radar system design and detection techniques of tracking and guiding radar.

XIA AI was born in Yulin, China, in 1986. He received the Ph.D. degree in electromagnetics and microwave technology from Xidian University, Xi'an, China, in 2013.

He is currently a Senior Engineer with the National Key Laboratory of Science and Technology on Test Physics and Numerical Mathematics. His research interests include computational electromagnetics, radar target recognition, and electromagnetic scattering characteristic of complex medium.

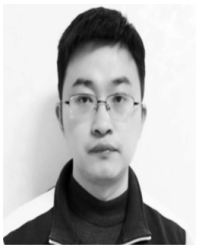

XIAOFENG AI was born in Ziyang, Sichuan, China, in 1983. He received the B.S. and M.S. degrees in electronic engineering and the Ph.D. degree in information and communication engineering from the National University of Defense Technology (NUDT), Changsha, China, in 2005, 2007, and 2013, respectively.

He is currently a Lecturer with NUDT. His research interests include radar imaging and feature extraction.

JIN LIU was born in Ganzhou, Jiangxi, China, in 1981. He received the B.S. degree in electronic engineering and the Ph.D. degree in information and communication engineering from NUDT, Changsha, China, in 2002 and 2010, respectively.

He is currently a Lecturer in with NUDT. His research interests include signal processing, radar target recognition, and radar imaging.

SHUNPING XIAO was born in Nanchang, Jiangxi, China, in 1964. He received the B.S. and Ph.D. degrees in electronic engineering from NUDT, Changsha, China, in 1986 and 1995, respectively.

He is currently a Professor with NUDT. His research interests include radar target recognition and radar signal processing.

Dr. Xiao is also a Senior Member of CIE.